International Immunopharmacology 122 (2023) 110545

Contents lists available at ScienceDirect

International Immunopharmacology

journal homepage: www.elsevier.com/locate/intimp

AT2 cell–derived IgA trapped by the extracellular matrix in silica-induced pulmonary fibrosis

Mengling Chen [a,1], Jing Wang [a,1], Mengqin Yuan [b,1], Min Long [b], Yuheng Sun [a], Sha Wang [a], Wei Luo [a], Yun Zhou [e], Wei Zhang [a], Wei Jiang [b,*], Jie Chao [a,c,d,*]

[a] Jiangsu Provincial Key Laboratory of Critical Care Medicine, Zhongda Hospital, Department of Physiology, School of Medicine, Southeast University, Nanjing, Jiangsu, China
[b] Department of Biomedical Engineering, Nanjing University of Aeronautics and Astronautics, Nanjing, Jiangsu, China
[c] Key Laboratory of Environmental Medicine Engineering, Ministry of Education, School of Public Health, Southeast University, Nanjing, Jiangsu, China
[d] School of Medicine, Xizang Minzu University, Xianyang, Shanxi, China
[e] Department of Health Management, School of Health Science, West Yunnan University of Applied Sciences, Dali, Yunnan, China

A B S T R A C T

Pulmonary fibrosis is an interstitial lung disease caused by various factors such as exposure to workplace environmental contaminants, drugs, or X-rays. Epithelial cells are among the driving factors of pulmonary fibrosis. Immunoglobulin A (IgA), traditionally thought to be secreted by B cells, is an important immune factor involved in respiratory mucosal immunity. In the current study, we found that lung epithelial cells are involved in IgA secretion, which, in turn, promotes pulmonary fibrosis. Spatial transcriptomics and single-cell sequencing suggest that *Igha* transcripts were highly expressed in the fibrotic lesion areas of lungs from silica-treated mice. Reconstruction of B-cell receptor (BCR) sequences revealed a new cluster of AT2-like epithelial cells with a shared BCR and high expression of genes related to IgA production. Furthermore, the secretion of IgA by AT2-like cells was trapped by the extracellular matrix and aggravated pulmonary fibrosis by activating fibroblasts. Targeted blockade of IgA secretion by pulmonary epithelial cells may be a potential strategy for treating pulmonary fibrosis.

1. Introduction

Pulmonary fibrosis is a chronic progressive disease causing changes in pulmonary interstitial components [1]. The extracellular matrix (ECM), a framework that supports lung tissue, is mainly composed of five proteins that are affected by lung cells and can, in turn, act on lung cells [2–3]. Lung epithelial injury and apoptosis are thought to be initiating factors in pulmonary fibrosis [4]. To maintain a normal alveolar structure, lung epithelial progenitor cells proliferate and differentiate to replenish alveolar epithelial cells [5–6]. Indeed, abnormal and excessive proliferation of progenitor cells fails to restore normal lung structure. Additionally, progenitor cells secrete various cytokines that affect fibroblasts [7]. Recent studies have indicated that dysregulated repair and regeneration of epithelial cells are a driving factor of lung fibrosis [8–10]. However, the specific molecular mechanisms used in the communication between the epithelium and other cells remain unclear.

Systematically, pulmonary fibrosis is related to the dysfunction of the immune system, and patients with autoimmune diseases suffer from pulmonary fibrosis to varying degrees [1]. Cellular and humoral immunity are two components of the immune system, and they can work both independently and in concert with each other [11]. In cellular immunity, T cells differentiate into effector T cells after being stimulated by antigens. They then combine and decompose the specific pathogenic microbes or cells [12]. In humoral immunity, B cells differentiate into effector B cells after being stimulated by antigens. Following this process, they produce specific antibodies that bind to the antigens on the invading microorganisms [13]. Variable (V), diversity (D), and joining

Abbreviations: BCR, B-cell receptor; CCK-8, Cell Counting Kit-8; CT, computed tomography; DEG, differentially expressed gene; ECM, extracellular matrix; FC, fold change; GEM, gel bead in emulsion; GO, Gene Ontology; IC, inspiratory capacity; IPF, idiopathic pulmonary fibrosis; KEGG, Kyoto Encyclopedia of Genes and Genomes; LC-MS, liquid chromatography mass spectrometry; MMEF, maximal mid-expiratory flow; NS, normal saline; PBS, phosphate-buffered saline; qRT-PCR, real-time quantitative; SLE, systemic lupus erythematosus; TRA, TCR α-chain; TRB, TCR β-chain; UMAP, uniform manifold approximation and projection.

* Corresponding authors at: Department of Physiology, School of Medicine, Southeast University, 87 Dingjiaqiao Rd, Nanjing, Jiangsu 210009, China (J. Chao). Department of Biomedical Engineering, College of Automation Engineering, Nanjing University of Aeronautics and Astronautics, 29 Jiangjun Avenue, Nanjing, Jiangsu, 211106, China (W. Jiang).

E-mail addresses: weijiang@nuaa.edu.cn (W. Jiang), chaojie@seu.edu.cn (J. Chao).

[1] M. Chen, J. Wang, and M. Yuan contributed equally to this paper.

https://doi.org/10.1016/j.intimp.2023.110545
Received 24 April 2023; Received in revised form 14 June 2023; Accepted 18 June 2023
1567-5769/© 2023 Published by Elsevier B.V.

(J) gene rearrangement of the T-cell receptor for antigen (TCR) and B-cell receptor (BCR) is an indispensable part of the differentiation process in T cells and B cells [14]. Single-cell sequencing allows us to understand the clonal amplification of T cells and B cells at the mRNA level and explore their relationships with diseases. There are five types of immunoglobulins, i.e., IgA, IgM, IgD, IgG, and IgE, of which IgA is the most abundant antibody on the mucosal surface [15].

IgA, which is distributed on the surfaces of mucosal membranes in the respiratory tract, can induce pulmonary fibroblasts to proliferate and produce inflammatory cytokines [16]. In patients with idiopathic pulmonary fibrosis (IPF), increased levels of autoreactive IgA correlate with disease progression [17]. Clinical studies have shown that elevated levels of IgA autoantibodies in the blood of patients with cystic fibrosis are associated with severe lung dysfunction [18–19]. However, there is also evidence that IgA, which affects lung function, is produced in the airways [20]. Molecular evidence for the origin of increased IgA presence in the lung is lacking, and where IgA is distributed to in the fibrotic lung has not yet been described.

In our present study, we investigated the involvement of pulmonary epithelial cells and IgA deposition in a silica-induced mouse model of pulmonary fibrosis. Then, we used spatial transcriptomics and single-cell sequencing to analyze the lung tissues obtained from silica-induced and control mice.

2. Materials and methods

2.1. Ethics statements

All animal experiments were approved by the Animal Care & Welfare Committee of Southeast University (approval number 20190121002). At the end of the experiments, the animals were humanely euthanized. All experimental procedures complied with the rules of animal experimental ethics. The animal experimental ethics committee supervised and inspected all experimental procedures.

2.2. Mice

Male C57BL/6 mice (6 weeks old) were purchased from Hangzhou Ziyuan Experimental Animal Company (Hangzhou, China). The mice were housed at three to five animals per cage, and were maintained at a stable temperature (22 °C ± 2 °C) and humidity (40% ± 10%), and at a 12:12-h light–dark cycle. The mice were allowed free access to water and provided with food at specified feeding times.

2.3. Establishment of a mouse model of pulmonary fibrosis via inhalation of silica

Silica particles having a diameter of 5 μm (80% of particles) were purchased from Sigma® (S5631). Silica particles were incubated at 180 °C for 16 h to inactivate the endotoxin. Silica was suspended in normal saline (NS) at 50 mg/ml to prepare a working solution. Male C57BL/6J mice (6 weeks of age, weighing 22 ± 1 g) were fasted, but provided with water, for 6 h before and after surgery. The mice were anaesthetized using pentobarbital sodium (1%, 50 mg/kg in ddH_2O) administered via intraperitoneal injection (ip). After the fur on the neck of each mouse was shaved, the skin was disinfected with 75% ethanol, and an incision (1 cm) was made on the skin along the midline. The soft tissue on the front of the neck was bluntly separated to expose the trachea. Mice in the SiO_2-7d and SiO_2-56d groups were administered 100 μl silica suspension (50 mg/ml) via intratracheal instillation into the lungs. Mice in the NS-7d and NS-56d groups were administered NS using the same delivery method. The area containing the incision on each mouse was sutured and disinfected, and the mice were closely observed until they had recovered from the procedure. The mice were observed every 8 h for the first 3 days after surgery, and once per day thereafter.

2.4. Computed tomography (CT)

Mice were anaesthetized using inhaled isoflurane (induction concentration 3–44%, maintenance concentration 1–1.5%). When the breathing of each mouse was deemed stable, the mouse was placed onto a mouse platform and scanned using Hiscan XM Micro CT (Suzhou Hiscan Information Technology Company; Suzhou, China) The X-ray tube settings were 60 kV and 133 μA, and images were acquired at a resolution of 50 μm. A 0.5° rotation step through a 360° angular range, with 50 ms exposure per step, was used. The images were reconstructed using Hiscan Reconstruct software (Version 3.0, Suzhou Hiscan Information Technology Company) and analysed with Hiscan Analyzer software (Version 3.0, Suzhou Hiscan Information Technology Co., Ltd.).

2.5. Pulmonary function tests

Mice were anaesthetized using an injection of pentobarbital sodium as described in the subsection entitled "**Establishment of a mouse model of pulmonary fibrosis via inhalation of silica**." Then, a tracheal catheter was inserted into, and fastened to, the trachea. For each mouse, a Forced Manoeuvres System (EMMS, Hants, UK) was then used to assess the following pulmonary functions: Cchord (Chord compliance between 0 and 10 cm H_2O); FEV75 (volume expired in the first 75 ms of fast expiration); IC (inspiratory capacity; volume inspired during slow inspiration); MMEF (mean mid expiratory flow; average flow between 25 and 75%); FVC (forced vital capacity, volume expired during fast expiration); and total lung capacity (FRC + IC). Each mouse was assessed three times, and the most reliable result was used for further analysis, while unusually high or low values were removed. The mice were then humanely euthanized, and lung tissues were harvested and stored at − 80 °C until further analysis.

2.6. Processing of mouse lung tissue for histology

Fresh lung tissues were immediately fixed in 4% paraformaldehyde and maintained at 4 °C for 24 h. For dehydration, the lung tissues were incubated overnight in 20% and then again overnight in 30% sucrose solution. Finally, the lung tissues were stored at − 80 °C until further use.

2.7. Haematoxylin and eosin (H&E) staining

Lung tissue tissues were sectioned at 8 μm at − 20 °C using a cryostat (Leica, Germany). The sections were then stained using an H&E staining kit (Biyun Tian, China) in accordance with the manufacturer's protocol. Briefly, tissue sections were washed three times in precooled phosphate-buffered saline (1 × PBS), stained with haematoxylin for 5 min, and then transferred into an acid alcohol fast differentiation solution for 10 s. The sections were soaked in tap water for 15 min, then stained with eosin for 5 min and washed under running water. Then, the sections were dehydrated in 75%, 95%, and 100% alcohol, and 100% xylene, for 1 min in each bath. Finally, neutral gum and glass slides were used to cover the tissue. After the sections were air dried, images were acquired at 10 and 20 × resolution using an EVOS FL AUTO2 Cell Imaging System (Thermo Fisher Scientific, Waltham, Massachusetts, USA). EVOS Automated Imaging System software (Thermo Fisher Scientific) was used specifically for the capture of images at 10 × resolution.

2.8. Sirius red staining

All tissue sections were stained using a Sirius Star Chromosome Kit (Abcam, USA) per manufacturer's protocol. Briefly, 8-μm thick lung tissue sections were washed in PBS three times for 5 min each time. The sections were then stained with Sirius red for 1 h and rinsed briefly using 1% acetic acid. Images were captured at 10 × and 20 × resolution using

an EVOS FL AUTO2 Cell Imaging System (Thermo Fisher Scientific). EVOS Automated Imaging System software (Thermo Fisher Scientific) was used specifically for the capture of images at 10 × resolution.

2.9. ECM processing and proteomic analysis

2.9.1. ECM collection

Fresh lung tissues were sectioned at 200 μm using a cryostat (Leica). The sections were rinsed using PBS and then incubated in 15 ml lysis buffer (1% SDS in ddH_2O) at 24–26 °C for 1 h on a shaker (Shanghai Yiheng Scientific Instrument Company; Shanghai, China). Then, the lung tissues were transferred into fresh lysis buffer and incubated at 24–26 °C for 1 h, after which they were transferred into new tubes containing fresh lysis buffer and incubated overnight at room temperature. On the following day, the tissues were incubated with 1% Triton X-100 (diluted using ddH_2O) at room temperature for 1 h; this incubation was repeated twice. Next, the tissues were placed into fresh 1% Triton X-100 solution and incubated overnight at room temperature. On the following day, the tissues were washed using PBS and then ddH_2O for 5 min each time at room temperature. The tissues were then incubated in a sodium chloride solution (1 M) for 1 h, and then washed using PBS followed by ddH_2O for 5 min each time at room temperature. Consequently, the tissues were incubated in a solution containing DNase (20 μg/ml) and $MgCl_2$ (4.2 mM) at 37 °C for 1 h. Finally, the tissues were washed with ddH_2O, membrane and nuclear proteins were extracted, and lung ECM was obtained.

2.9.2. Extraction of ECM proteins

Lung ECM was added to an appropriate amount of SDS lysis buffer (Biyun Tian, China), incubated at 37 °C for 1 h, and centrifuged at room temperature and at 121,130*g* for 15 min. The supernatant was collected and designated as ECM protein solution, which was stored in PBS at 4 °C until use.

2.9.3. Proteomic analysis of the ECM

Total protein was extracted from the following six samples of lung ECM: three samples for the NS-56d group of mice (samples designated as con111, con116, and con117), and three samples for the SiO_2-56d group of mice (samples designated as M80, M101, and M107). First, each 10-μl sample was used for the assessment of protein concentration using a BCA kit (Biyuntian; Wuhan, China) and a fluorospectrophotometer (Horiba; Kyoto, Japan), after which the proteins were separated using SDS-PAGE. Then, 50 μg protein was collected for trypsin digestion and labelled using Tandem Mass Tags reagents as follows: con111 labelled with 126, con 116 with 127, con117 with 128, M80 with 129, M101 with 130, and M107 with 131. Equal amount of each labelled sample was vortexed, and 120 μl peptide solution was used for chromatographic separation. Finally, the samples were analysed using liquid chromatography mass spectrometry (LC-MS).

2.10. Western blotting

The proteins were boiled in loading buffer at 100 °C for 5 min. Then, 20 μg protein obtained from lung ECM was loaded onto to a 12% SDS-PAGE gel and subjected to separation. The proteins were then transferred to a 0.25-μm PVDF membrane, and the membrane was incubated in 5% skim milk at room temperature for 1 h to block nonspecific binding sites. Then, the membranes were incubated with the primary antibody (anti-pro/mature surfactant protein B, ab40876, Abcam, 1:5000) at 4 °C overnight. After being washed four times with TBST at room temperature for 8 min, the membranes were incubated with an HRP-conjugated Affinipure Goat Anti-Rabbit IgG (H + L) (Proteintech; Rosemont, IL, USA) for 1 h at room temperature. For the detection of IgA, goat anti-mouse IgA-HRP (Southern Biotech, SBA-1040-05, 1:5000) was used as both the primary and secondary antibody. After unbound secondary antibodies were fully washed off using TBST, signals were detected using an Immobilon ECL Ultra Western HRP Substrate (Millipore; Burlington, MA, USA), and images were acquired with a chemiluminescence detection system (Tanon Scientific & Technology Co.; Shanghai, China). For lung ECM samples, β-actin was used as an internal reference protein. For MLE-12 samples, GAPDH was used as an internal reference protein.

2.11. Spatial transcriptomics

2.11.1. Sample collection

If obvious fibrotic lesions in the mouse lungs were visible on CT imaging, the mouse model of pulmonary fibrosis via silica instillation was designated as having been successfully established. Lung tissues were trimmed near the hilum in the horizontal direction and were immediately frozen in OCT on dry ice. Tissues were then stored at −80 °C until further use.

2.11.2. Staining and imaging

Cryosections were cut at 10-μm thickness using a cryostat (Leica) and mounted onto GEX arrays. The arrays were placed on a Thermocycler Adaptor with the active surface facing up, and were then incubated for 1 min at 37 °C, fixed for 30 min using methyl alcohol at −20 °C, and stained with H&E. Bright-field images of the whole slide were acquired using a Leica DMI8 whole-slide scanner at a resolution of 10×.

2.11.3. Permeabilization and reverse transcription

Spatial gene expression analysis was performed using the Visium Spatial Gene Expression Slide and Reagent Kit (10x Genomics, PN-1000184). A Visium slide cassette was used to create leak-proof wells for adding reagents. Then, 70 μl permeabilization enzyme was added, and the samples were incubated at 37 °C. Samples SiO_2-7d, NS-7d, and NS-56d were incubated for 24 min. Because of severe lung fibrosis, samples obtained from the SiO_2-56d group of mice were incubated for 30 min. Each well was washed with 100 μl saline sodium citrate buffer, and then 75 μl RT master mix was added for cDNA synthesis performed using the following parameters: 65 °C for 15 min, and held at 4 °C.

2.11.4. cDNA library preparation for sequencing

After first-strand synthesis, RT Master Mix was removed from the wells. Then, 75 μl 0.08 M KOH was added to each well, and the wells were allowed to incubate for 5 min at room temperature. KOH was then removed from the wells, and the wells were washed using 100 μl EB buffer. Then, 75 μl Second Strand Mix was added to each well for second-strand synthesis. cDNA amplification was performed on a S1000TM Touch Thermal Cycler (Bio-Rad) under the following conditions: 98 °C for 3 min, 98 °C for 15 s, 63 °C for 20 s, 72 °C for 1 min, 14 cycles; 72 °C for 1 min, and held at 4 °C. Visium spatial libraries were constructed using a Visium spatial library construction kit (10x Genomics, PN-1000184) according to the manufacturer's instructions. The libraries were sequenced using an Illumina NovaSeq6000 sequencer with a sequencing depth of at least 100,000 reads per spot with a paired-end 150-bp reading strategy (performed by CapitalBio Technology, Beijing, China).

2.12. Single-cell sequencing of mouse lung tissue

2.12.1. Sample collection

For mice instilled with SiO_2 suspension, only mice with obvious high-density shadows visible on CT imaging were included. Lung samples for single-cell sequencing were collected from mice in the four mouse groups (SiO_2-7d, NS-7d, SiO_2-56d, and NS-56d). Whole lungs were removed from each mouse within 2 min of euthanasia and quickly washed in precooled PBS three times.

2.12.2. Cell capture and cDNA synthesis

Whole lung tissue was cut into approximately 10-mm pieces and

dissociated into single cells using a Lung Dissociation Kit (Miltenyi Biotech, 130-095-927, Germany). Using Single-Cell 5′ Library and Gel Bead Kit (10x Genomics, 1000169) and Chromium Single-Cell G Chip Kit (10x Genomics, 1000120), a cell suspension (300–600 living cells per μl as determined by CountStar) was loaded onto a Chromium single-cell controller (10x Genomics) to generate single-cell gel beads in emulsion (GEMs) according to the manufacturer's protocol. In short, single cells were suspended in PBS containing 0.04% BSA. Approximately 20,000 cells were added to each channel, and target cell recovery was estimated to be approximately 10,000 cells. Captured cells were lysed, and the released RNA was barcoded using reverse transcription in individual GEMs. Reverse transcription was performed on a S1000TM Touch Thermal Cycler (Bio-Rad) at 53 °C for 45 min, followed by 85 °C for 5 min, and then held at 4 °C. cDNA was generated and then amplified, and cDNA quality was assessed using an Agilent 4200 system (performed by CapitalBio Technology, Beijing).

2.12.3. ScRNA-seq library preparation

ScRNA-seq libraries were constructed using Single-Cell 5′ Library and Gel Bead Kit (1000165), Single Cell V(D)J Enrichment Kit, Mouse T Cell (1000071), and Single Cell V(D)J Enrichment Kit, Mouse B Cell (1000072) according to the instructions of each manufacturer. The libraries were sequenced using an Illumina NovaSeq6000 sequencer with a sequencing depth of at least 100,000 reads per cell with a paired-end 150-bp reading strategy (performed by CapitalBio Technology, Beijing).

2.13. RNAscope

2.13.1. Preparation of lung tissue sections

Lung tissues harvested from SiO_2-56d and NS-56d mice were immediately frozen in OCT on dry ice and then stored at − 80 °C until further use.

2.13.2. RNAscope in situ hybridization

All RNAscope assays (ACD) were performed in accordance with the manufacturer's instructions. The tissues were equilibrated at −20 °C for 1 h, sectioned at 12 μm using a cryostat (Leica, Germany) at −20 °C, and mounted onto SuperFrost Plus slides (Fisher, Scientific, 12-550-15). Tissue sections were air-dried at −20 °C for 20 min and then immediately transferred into 4% paraformaldehyde (precooled at 4 °C) for 15 min. Next, the tissue sections were dehydrated by submerging once in 50% and then in 70% ethanol, and twice in 100% ethanol, at room temperature, for 5 min in each bath. The sections were then air-dried for 5 min, and the boundaries of the sections were drawn on the slides using an ImmEdge hydrophobic pen. After the hydrophobic boundaries had dried, the tissue sections were incubated in a hydrogen peroxide solution for 10 min, and then briefly washed twice in PBS. Next, the tissue sections were incubated with protease IV for 15 min at room temperature followed by two brief washes in PBS.

The tissue sections were placed into a humidity box and incubated with a solution containing an *Sftpc* probe (C3, 570) and an *Igha* probe (C2, 520) (1:50 diluted in probe diluent) at 4 °C for 2 h. The tissue sections were then washed twice in 1× washing buffer at room temperature for 2 min. Consequently, the tissue sections were incubated with AMP-1, AMP-2, and AMP-3 for 30, 30, and 15 min, respectively, at 40 °C. After each amplification, the sections were washed twice in 1× washing buffer at room temperature for 2 min. Next, the sections were incubated with HRP-C2 at 40 °C for 15 min, and then washed twice in 1× washing buffer at room temperature for 2 min. Then, the sections were incubated with Opal 520 (1:1000 diluted in TSA diluent) at 40 °C for 30 min, followed by two washes in 1× washing buffer at room temperature for 2 min. The sections were then incubated with HRP-C3 at 40 °C for 15 min, followed by two washes in 1× washing buffer at room temperature for 2 min. Next, the sections were incubated with Opal 570 (1:1000 diluted in TSA diluent) at 40 °C for 15 min, and then washed twice in 1× washing buffer at room temperature for 2 min. Finally, the sections were incubated with DAPI for 30 s. After a brief wash in PBS, the sections were mounted using Prolong Gold Antifade mounting medium (Thermo Fisher Scientific, P36930, USA). All the slides were fully air-dried and then stored in the dark at 4 °C.

2.13.3. Image capture

Images were captured using a confocal microscope (Olympus FV1000, Japan). The overall morphology of each sample was observed using a 10× objective lens. Detailed images were acquired using a 60× objective oil lens. Images of different channels were acquired separately and merged using Olympus Fluoview software.

2.14. Cell culture

MLE-12 cells (mouse lung epithelial cells, ATCC number: CRL-2110) were cultured in DMEM (Gibco) supplemented with 10% FBS (Corning) and 1% penicillin–streptomycin (Gibco) in an incubator (Thermo) at 5% CO_2 and 37 °C.

2.15. Protein extraction

Cells were washed three times with precooled PBS, lysed using RIPA lysis buffer (Beyotime Biotechnology, China) supplemented with a protease inhibitor cocktail (Beyotime Biotechnology, China) on ice for 1 h, and then centrifuged at 13,523*g* for 15 min. Protein concentration in the supernatants was quantified using a BCA assay (Beyotime Biotechnology, China). The extracted protein was heated for 5 min at 100 °C and then cooled on ice for 5 min, and the protein solution was stored at −80 °C.

2.16. Real-time quantitative PCR

Real-time quantitative PCR (qRT-PCR) was used to detect the relative expression level of *Igha* mRNA (primer: F: AACCTGAGGACAGCAGGGTT, R: ATACCTCCCTAAACCCCAGTTC). First, TRIzol (Invitrogen, USA) was used to extract total RNA from MLE-12 cells following the manufacturer's protocol. Then, mRNA concentration in each sample was measured using a NanoDrop One Microvolume UV–Vis Spectrophotometer (Thermo Fisher Scientific). mRNA concentration was then normalized for each sample, and DNA contamination was removed using a genomic DNA wiper. For each sample, an equivalent amount of mRNA was reversed-transcribed into cDNAs using a HiScript Q RT SuperMix for qPCR Kit (Vazyme; Dover, DE, USA); the expression levels of target genes were then analyzed using a SYBR Green Real-time PCR Master Mix (Vazyme) and an Applied Biosystems Real-time PCR System according to the manufacturer's instructions. PCR efficiency (E) calculated from the slope and r^2 of calibration curve were as follows: $90\% < E < 105\%$ and $r^2 > 0.980$.

2.17. CCK-8 assay

A Cell Counting Kit-8 (CCK-8) (Apexbio; Houston, TX, USA) was used to detect cell proliferation in accordance with the manufacturer's instructions.

2.18. Migration assay

MLg-GFP cells were seeded onto the ECM obtained from mice in each experimental group, and images were acquired at 24, 48, and 72 h of culture using an EVOS FL AUTO2 Cell Imaging System (Thermo Fisher Scientific) at a resolution of 10×.

2.19. Statistical analyses

2.19.1. Analysis of LC-MS/MS data

The LC-MS/MS raw data were processed using Proteome Discover

2.4 (Thermo, USA). According to the unique peptide ≥1, any group of samples with the expression value ≥50% of the protein were retained. Then, the missing values were imputed with the mean of protein expression in the corresponding group. Credible proteins were obtained using median normalization and log2 logarithmic conversion of protein abundance data. Statistical analysis was performed using the R software (version 4.2) and protein visualisation was performed using ggplot2 package (version 3.2.2), and the following analyses were performed: principal component analysis, sample correlation analysis, sample hierarchical cluster analysis, visual display of data after standardization, and density plotting.

Based on the obtained credible proteins, Student's *t* test was used to identify significant differences between proteins in the NS-56d group and those in the SiO_2-56d group of mice. Fold change (FC) was used to evaluate differences in protein expression levels among the samples. P-value (P) calculated using Student's *t*-test was used to indicate statistically significant differences between the groups. Screening threshold was log FC ≥ 1.0 and P ≤ 0.05. A clustering heatmap constructed using R software (version 4.2) was used for quality control and display of standardized experimental data after enrichment of differential data. Generally, samples of the same group can appear in the same cluster. For the identified proteins, extraction of the annotation information was based on Uniprot databases. After obtaining the differentially expressed proteins (FC ≥ 2, P ≤ 0.05), GO and KEGG functional enrichment analyses of the upregulated proteins were performed using the R software (version 4.2).

2.19.2. Analysis of scRNA-seq data

The original data of scRNA-seq has been uploaded to GEO database (GSE number in GEO datasets: GSE183682). Cell barcode filtering, alignment of reads, and UMI counting were performed using Cell Ranger 4.0.0 (https://www.10xgenomics.com/). The number of cells was estimated and recorded as N according to the cell capture rate (50%–65%) using Chromium TM Single Cell Gene Expression Solution. Then the 99th percentile of UMI quantity of the first N barcodes was calculated and recorded as Y in descending order of UMI quantity. Barcodes that met the inclusion criterion (UMI quantity > Y × 10%) were directly classified as effective cells. Barcodes with low UMI content were considered empty GEMs and used to establish a background model. If any given barcode whose number of UMIs < Y × 10% was significantly different from the background, it would be added to the effective cell set. scRNA-seq data for the four mouse groups were combined using Cell Ranger aggr. Normalized data were subjected to principal component analysis. Unsupervised clustering was performed using Cell Ranger reanalysis with a graph-based algorithm. The top 10 principal components were used for clustering and uniform manifold approximation and projection (UMAP). The differential expression of genes among clusters was computed using Cell Ranger 4.0.0. Pseudotime analysis was carried out with the Monocle R package. GO and KEGG functional enrichment analyses of marker genes (FC ≥ 2, P ≤ 0.05) in clusters 1 and 6 were performed using Metascape (https://metascape.org).

2.19.3. Cell type annotation

Cell types were determined using clustering and marker gene expression. Cells in clusters 1, 3, and 15 highly expressed the genes *Sftpc*, *Sftpb, Sftpd*, and *Sftpa1*, and were defined as AT2-like cells. Cluster 6 cells highly expressed the genes *Itgax*, *Csf1r*, and *Ly86*, and were inferred to be macrophages. Monocytes were contained in clusters 4 and 8, which highly expressed *Ccr2* and *Csf1r*. Other clusters were highly expressed markers specific for dendritic cells (*Ear1* and *Plet1*), Club cells (*Sftpb*, *Sftpc*, and *Scgb3a1*), AT1 cells (*Cldn3* and *Epcam*), Ccl3 − Ccl4 − neutrophils (*Cxcr2* and *Stfa2l1*), Ccl3 + Ccl4 + neutrophils (*Il1f9*, *Ccl3*, and *Ccl4*), T cells (*Thy1* and *Cd8a*), B cells (*Cd79a*, *Cd79b*, and *Cd19*), endothelial cells (*Cdh5*, *Pecam1*, and *Clec14a*), fibroblasts (*Col1a1*, *Col3a1*, and *Col6a2*), and red blood cells (*Hba-a1* and *Hba-a2*).

2.19.4. BCR and TCR sequence reconstruction

Using a Chromium Single-Cell V(D)J Enrichment kit, we reconstructed full-length TCR/BCR V(D)J segments from amplified cDNA in 5′ libraries from PCR amplification of sc-RNA seq following the manufacturer's protocol (10x Genomics). Using the Cell Ranger (v.4.0.0) vdj pipeline coupled with the mouse reference genome mm10, we performed demultiplexing, gene quantification, and TCR/BCR clonotype assignment. Cells with at least one complete TCR α-chain (TRA) or TCR β-chain (TRB) were retained for TCR analysis, and only cells with at least one complete heavy chain (IGH) or one light chain (IGK or IGL) were retained for BCR analysis. Each unique TRA(s)-TRB(s) pair or IGH(s)-IGK/IGL(s) pair was defined as an effective clonotype for further clonal expansion analysis. Cells with the same clonotype were considered clonal cells. Based on barcode information, cells with a TCR or BCR clonotype were projected using UMAP plots.

2.19.5. Analysis of spatial transcriptomics data

The original data of spatial transcriptomics has been uploaded to GEO database (GSE number in GEO datasets: GSE183683). First, 10X Space Ranger software, which can process, align, and summarize UMI counts against the mmu10 mouse reference genome for each spot, was used to generate a feature-barcode matrix. Only spots overlaying the tissue sections were retained for further analysis. Unsupervised clustering was based on a graph-based algorithm with 10 principal components. UMAP was performed to visualize the spots in a two-dimensional space. Spatial feature expression plots were generated using Loupe Browser 4.1.0.

2.19.6. scRNA-seq and spatial RNA-seq integration

To obtain the composition of cell types in each spot, we used anchor-based integration method in Seurat v3.2, which can transfer the label of an scRNA-seq reference to a spatial RNA-seq query. First, the data obtained using scRNA-seq and spatial RNA-seq were normalized using the SCTransform function. Then, cell type prediction probability scores were calculated for each spot using FindTransferAnchors and TransferData functions. Finally, a spot was assigned to the cell type having the highest score.

2.19.7. Assessment of significant differences between groups

GraphPad Prism 8 Software was used for statistical analysis. Student's *t*-test was used to assess the significance of differences between two groups. Differences between two groups were considered significant at P < 0.05.

3. Results

3.1. Single-cell sequencing detects highly amplified expression of AT2-like cells in the lungs of SiO_2-56d mice

Pneumoconiosis is a type of pulmonary fibrosis caused by inhalation of free silica. In our present study, we established a mouse model of lung fibrosis using intratracheal instillation of a silica suspension (SiO_2 group: 50 mg/ml, 100 μl); the mice in the control group received normal saline (NS group: 100 μl) instilled using the same method. Our results of computed tomography (CT) and hematoxylin and eosin (H&E) staining showed acute inflammation at 7 days after instillation in the SiO_2 group of mice; collagen deposition was observed in the lungs of these mice at 28 days after SiO_2 instillation, consistent with the results shown in previous studies that used this model [21–22]. At 56 days after instillation, the levels of several indicators of pulmonary function, including those of volume expired in the first 75 ms of fast expiration (FEV75), inspiratory capacity (IC), and maximal mid-expiratory flow (MMEF), were decreased in the lungs of SiO_2 mice (Fig. S1 A). In addition to the strip- or sheet-like areas of hyperdensity visible on CT (Fig. S1 B), higher values of lung coefficients (lung weight/mouse bodyweight) (Fig. S1, C and D) and collagen deposition detected using Sirius red staining

(Fig. S1 E), were present in the lungs of SiO_2-56d mice than in NS-56d mice. These results indicate that SiO_2 mice had entered the fibrotic stage at 56 days after instillation of the SiO_2 suspension (Fig. 1 A).

Whole lungs, obtained from the mice in the four groups (SiO_2-7d, NS-7d, SiO_2-56d, and NS-56d), were evaluated using scRNA-seq. All the mice in the four groups were scanned using CT prior to tissue collection to confirm that the SiO_2-instillation model of lung fibrosis had been successfully established (Fig. 1 B). Transcriptomic data, obtained from the analysis of mice in the four groups, were normalized, after which the combined cells from all groups were subjected to graph-based clustering, which yielded 24 cell clusters [23]. The cell type for each cluster was annotated according to canonical cell markers from CellMarker [24]. These 24 clusters were then sorted to 12 types of cells as presented in the uniform manifold approximation and projection (UMAP) diagram (Fig. 1 C and Fig. S1 F): endothelial cells, monocytes, macrophages, dendritic cells, B cells, T cells, neutrophils (*Ccl3*$^-$ *Ccl4*$^-$ neutrophils, *Ccl3*$^+$ *Ccl4*$^+$ neutrophils), fibroblasts, and Club cells, AT2-like cells (cluster 1, cluster 3, and cluster 15), red blood cells, and AT1cells. Pseudotime analysis indicated that cells of clusters 1, 3, and 15 constituted a developmental trajectory, indicating that they were at different stages of differentiation (Fig. S2 G).

To explore the cellular compositions of different samples, we calculated the relative percentages of the 12 main cell types and 3 AT2-like cell subsets in the mice of our four mouse groups (Fig. 1, D–H and Fig. S1 H). The relative percentage of macrophages in SiO_2-7d mice was markedly increased compared with that of NS-7d mice, representing up to 18% of the total number of cells; the percentage of macrophages in the SiO_2-56 mice was also higher than that in the NS-56d mice (Fig. 1 D). This finding indicates that macrophages were major participants in the inflammatory stage and were still present in the fibrotic stage. Gene Ontology (GO) and Kyoto Encyclopedia of Genes and Genomes (KEGG) analyses of differentially expressed genes (DEGs) in macrophages identified issues classically involved in the development of silicosis, such as inflammatory response, lytic vacuole, ATPase activity coupled to transmembrane movement, and lysosomes [25] (Fig. S2, A–D). *Ccl3*$^+$ *Ccl4*$^+$ neutrophils, which are often involved in various inflammatory reactions induced by bacteria, viruses, and foreign objects [26], were activated 7 days after stimulation using silica, and they were still detected until day 56 post-stimulation (Fig. 1 E).

Because cells in clusters 1, 3, and 15 expressed *Sftpc*, *Sftpb*, *Sftpd*, and *Sftpa1*, we designated the cells in these three clusters as AT2-like cells. The proportion of AT2-like cells in clusters 1 and 15 was increased; however, cluster 15 had less AT2-like cells than cluster 1 (Fig. 1, F–H). Interestingly, the proportion of AT2-like cluster 1 cells in the SiO_2-56d mice was notably increased, reaching 40% (Fig. 1 F), which may play an important role in fibrosis. This finding indicates that the newly discovered AT2 cell subsets, namely AT2-like cluster 1 cells, increased in number when inflammation had slightly subsided in progressive pulmonary fibrosis.

3.2. scRNA-seq and spatial transcriptomics indicate that the number of AT2-like cluster 1 cells is increased in the SiO_2-56d mice

To further explore the spatiotemporal characteristics of transcription in our murine model of lung fibrosis, we analysed the four mouse groups (NS-7d, SiO_2-7d, NS-56d, and SiO_2-56d) using spatial transcriptomic sequencing. To obtain transcripts from the same structures, and to eliminate the potential confounding factors stemming from differences in anatomical location, we collected the left lung from each mouse and sectioned it horizontally (Fig. S2 E). Before sequencing, all mice were scanned using CT (Fig. S2 F) to verify that the mouse model of silica-induced pulmonary fibrosis had been established successfully. Our results show that both SiO_2-7d and SiO_2-56d mice exhibited hyperdense areas on their lungs, indicating that our model of pulmonary fibrosis had indeed been successfully established. During sectioning, lung tissues were evaluated using microscopy (Leica DMI8, Germany). If the hilum of the lung and left main bronchus were observed, the tissue section was mounted onto spatial transcriptomics arrays. Using this approach, we obtained four lung sections (one per each experimental group) having approximately the same shape and anatomical location, with the major vessels and hilum of the lung clearly visible. H&E staining showed that alveoli in the lungs of NS-7d and NS-56d mice had a normal structure with no infiltration of inflammatory cells (Fig. 1 I, top). The lungs of SiO_2-7d mice showed an accumulation of inflammatory cells and complete destruction of alveolar structures. In the lungs of SiO_2-56d mice, some alveoli were filled with neutrophils; infiltration of inflammatory cells was also detected, but was weaker than that in the lungs of SiO_2-7d mice (Fig. 1 I, top). This finding indicates that SiO_2-7d and SiO_2-56d mouse models of fibrosis were successfully established.

After assessing the basic histology of the lung sections in each group of mice, we performed spatial transcriptomic sequencing of the lung tissues collected from the mice in the four groups to obtain a total of 6778 spots (a single spot can hold cells within a 60-μm diameter). We then performed graph-based clustering to capture 11 clusters of spots (Fig. S2, G and H). Our results indicate that the lung tissues obtained from NS-7d and NS-56d mice were highly consistent in terms of clusters of spots (Fig. S2, I and J). Spot clustering in the SiO_2-7d and SiO_2-56d mice differed significantly from their respective controls; additionally, spot clustering in the SiO_2-7d mice differed significantly from that in the SiO_2-56d mice (Fig. S2, I and J). These findings indicate that mRNA expression at the same anatomical location changed substantially from the inflammatory stage (7d) to the fibrotic stage (56d).

To further investigate the location of cluster 1 cells in relation to fibrotic lesions in the lungs, we used Seurat V3.2 to integrate our datasets based on anchor features. We then predicted the main cell types included in the spatial transcriptional spots in the four sections, each section obtained from SiO_2-7d, NS-7d, SiO_2-56d, and NS-56d mice (Fig. S2 K). All 15 cell types (Fig. S1 F) identified using single-cell sequencing were predicted in the four sections obtained from SiO_2-7d, NS-7d, SiO_2-56d, and NS-56d mice. The scattering of different cell types across the four groups did not show any obvious pattern (Fig. 1 I, middle); this lack of an obvious pattern differed from the brain and kidney sections obtained from mice examined in previous studies, in which specific cell clusters were associated with a particular anatomical location [27–28]. Expectedly, macrophages were more densely clustered in the SiO_2-7d mouse lungs than in NS-7d mouse lungs (Fig. S2 L); this finding was consistent with the findings obtained using scRNA-seq, which also showed increased macrophage numbers in the SiO_2-7d mouse lungs compared with those in the NS-7d mouse lungs (Fig. 1 D). Similarly, AT2-like cluster 1 cells were present at a greater density in the lung lesions of SiO_2-56d mice than in the lungs of NS-56d mice (Fig. 1 I, bottom). Notably, B cells in the lungs of SiO_2-56d mice showed no particular pattern of distribution (Fig. S2 M). From a spatial perspective, this result verified that macrophages participated in silicosis, especially in the early stage, and that AT2-like cluster 1 cells played an important role in the fibrotic stage.

3.3. AT2-like cluster 1 cells acquire BCR genes

GO and KEGG analyses showed that 20 upregulated genes (FC greater than 2, $P < 0.05$) in AT2-like cluster 1 cells were enriched in immune-related terms such as systemic lupus erythematosus, circulating immunoglobulin complex, humoral immune response, and immunoglobulin production (Fig. 2, A–C). Thus, we hypothesized that AT2-like cluster 1 cells played an important role during the fibrotic stage. *Igha*, the gene encoding constant region of the IgA heavy chain, showed particularly high expression in cluster 1 in this mouse group (Fig. 2 D). To gain further insight into the function of cluster 1, we compared the DEGs in this cluster with those in all other cell clusters. We found that *Igkv13-85*, *Ighv3-6*, and *Igkv6-32* were the top three DEGs in AT2-like cluster 1 cells (Fig. 2, E–G). These three DEGs belonged to the V gene group, with *Igkv13-85* and *Igkv6-32* encoding the mouse

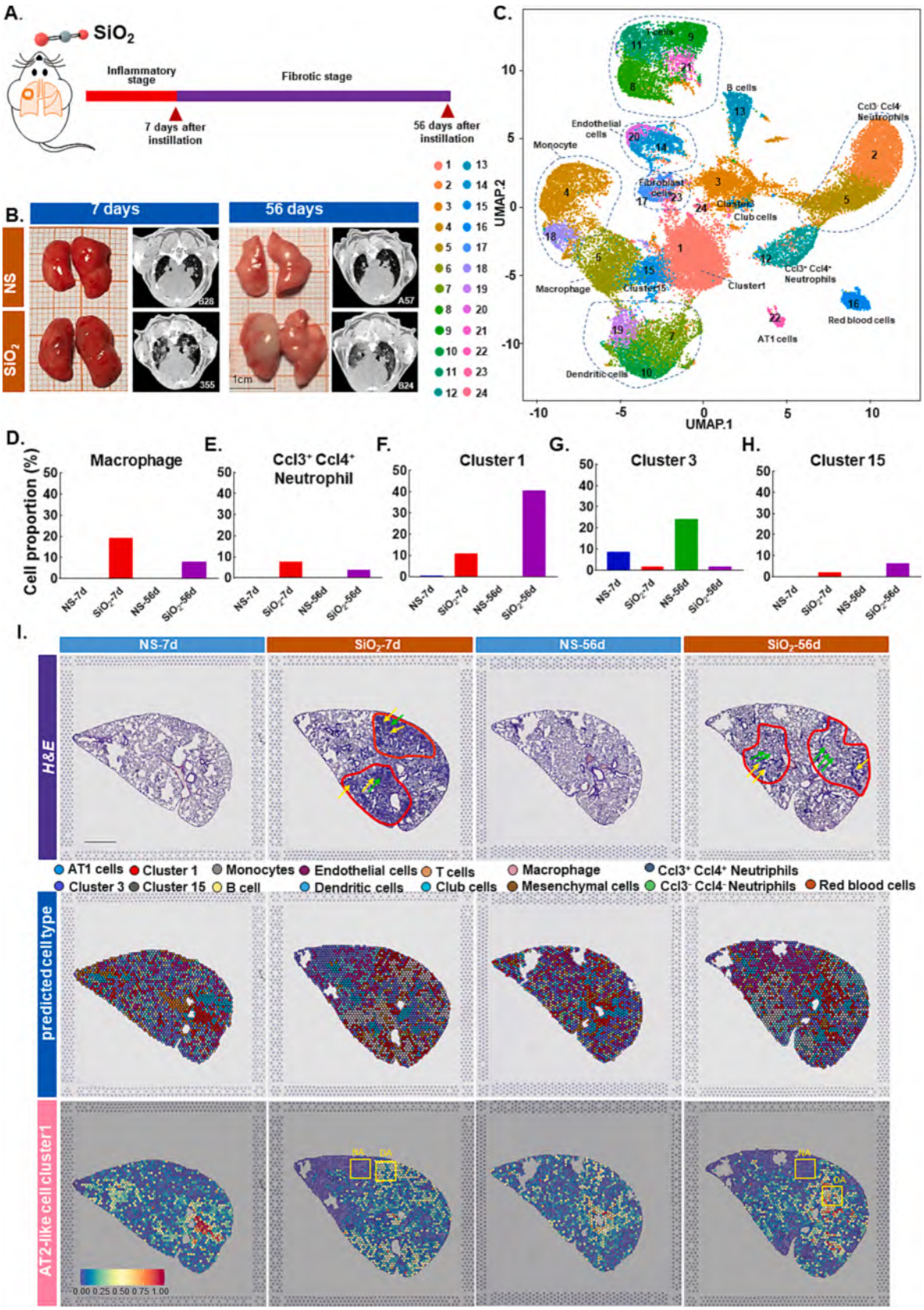

(caption on next page)

Fig. 1. AT2-like cluster 1 cells are amplified in SiO_2-56d mice and predicted to congregate in lesion areas. (A) Scheme of the study design. SiO_2-7d mice were used to represent the inflammatory stage, and NS-7d mice were used as controls. SiO_2-56d mice were used to represent the fibrotic stage, and NS-56d mice were used as controls. scRNA-seq was used to analyse the lung cells in the four groups of mice. **(B)** Images of fresh lung and chest CT are shown. **(C)** UMAP containing 43,397 single cells from SiO_2-7d, NS-7d, SiO_2-56d, and NS-56d mice. A single point represents a single cell. Each of the 24 clusters is marked with a specific colour. NS-7d mice were instilled with normal saline for 7 days; SiO_2-7d mice were instilled with silica suspension for 7 days; NS-56d mice were instilled with normal saline for 56 days; SiO_2-56d mice were instilled with silica suspension for 56 days. **(D–H)** Components of related cell types at 7 and 56 days. X axis, different samples; y axis, proportion of a certain cell type to total number of cells in a single sample. **(I)** Top, hematoxylin and eosin (H&E) staining of lung sections. Scale bar = 1 mm. Areas within the red lines are lesions. The yellow arrow indicates the exudation of inflammatory cells and the green arrow the change of alveolar structure. Middle, predicted distribution of 12 cell types and 3 AT2-like cell subsets in the four samples. Different colours represent corresponding cell types. Bottom, heatmaps show scores for AT2-like cluster 1 cells on each spot. NA, normal alveolar; DA, diseased alveolar; T-testing was used to compare the proportion of AT2-like cluster1 cells in DA and NA spots. The proportion of AT2 like cluster1 cells in DA was found to be significantly higher than that in NA.

immunoglobulin light, and *Ighv3-6* encoding the heavy, chain [29]. These three genes showed high expression levels in the SiO_2-56d mice and were mainly expressed in cluster 1 cells (Fig. 2 E–G).

In order to explore inflammation and fibrosis in across time, we analyzed mRNA levels of several factors relevant to inflammation and fibrosis. Spatial transcriptomics indicated that the inflammatory factors *Ccl2* and *Il6* (Fig. 2 H), fibrosis factors Fn1 and *Tgf-β1* (Fig. 2 I) were highly expressed in the lung lesions of SiO_2-7d mice, but showed decreased expression in the lung lesions of SiO_2-56d mice; this finding indicates decreased levels of inflammation but a certain degree of maintenance of fibrosis factors in SiO_2-56d mice. *Igha* and *Jchain,* which are related to the secretion of IgA [30], were highly expressed in the lung lesions of SiO_2-56d mice (Fig. 2 J); this finding indicates that production of IgA was increased in in-situ lung tissue. The expression of genes such as *Igkc* and *Iglc2*, encoding immunoglobulin light chains, was high in the lung lesions of SiO_2-56d mice (Fig. 2 K). This finding suggests that the expression of BCR genes may play an important role in the fibrotic stage.

3.4. BCR clonal expansion in the SiO_2-56d group of mice

Because spatial transcriptomics and single-cell sequencing showed differential expression of genes encoding the immunoglobulin light chain in the lung tissues of SiO_2-56d mice, we further explored the usage of V(D)J and C genes of the BCR of the mice of our four groups. For this, we reconstructed the BCR sequences from scRNA sequencing. Across the four groups, several V genes, including *Ighv1-64*, *Igkv13-85*, *Ighv3-6*, *Igkv6-32*, and *Igkv17-127*, were found at higher frequencies in the SiO_2-56d mice (Fig. 3, A and B). Among these five genes, *Igkv13-85*, *Ighv3-6*, and *Igkv6-32* were categorized as highly expressed DEGs in the AT2-like cell cluster 1 (Fig. 2, E–G). *Ighv1-64* and *Igkv17-127* were also mainly expressed in the AT2-like cell cluster 1 (Fig. 3, C and D). Among the IGH C genes, the expression of *Igha* was substantially increased in the SiO_2-56d mice compared with those in the other three groups of mice (Fig. 2 D); this increase in the expression of *Igha* indirectly led to a decline in the proportion of *Ighm* and *Ighd* usage (Fig. 3 E). There were no obvious differences in the usage of other BCR genes across the four mouse groups (Fig. S3, A–D).

Clonal expansion is closely related to disease progression. Our analysis of the top 30 clonotypes in each mouse group indicated no identical clonal expansion among the four mouse groups (Fig. S3, F–I). For the SiO_2-56d mice, a heatmap composed of different V-J gene pairing frequencies shows nine types of V-J combinations in clonal populations that had expanded to over 100 cells (Fig. S3, J–M). For the SiO_2-56d mice, clonotypes comprising over 100 cells constituted more than 75% of the total clonal cell population (Fig. 3 F); additionally, approximately 75% of the total clonal cells were AT2-like cluster 1 cells (Fig. S3 N). Combined with the results obtained using scRNA sequencing, these findings show that BCR genes were expressed not only in B cells but also in AT2-like cluster 1 cells. Indeed, more BCR^+ cells were identified as AT2-like cluster 1 cells (Fig. 3 G). At least half of the clonal cells were identified as AT2-like cluster 1 cells using scRNA barcodes (Fig. 3 H). These clones, expressing IGK and IGHA, produced IgA with the progression of pulmonary fibrosis (Fig. S3 E). To determine from which cell cluster these clones were derived, we merged the barcodes of the top three clonal cell populations with the barcodes from single-cell sequencing. Our results indicate that most of these clonal cells were AT2-like cluster 1 cells (Fig. 3 I). Cells having the top 1 clonotype highly expressed *Sftpc* and *Scgb3a1* compared with the levels of B cells (Fig. S3 O), indicating that cells in this cluster had a closer relationship with AT2 cells than with B cells.

3.5. Immunoglobulin-producing AT2-like cluster 1 cells possess more characteristics of AT2 cells than those of B cells

These genes (*Igkv13-85*, *Igkv6-32*, and *Ighv3-6*), which showed a highly differential expression in cluster 1, usually code for immunoglobulin and are expressed by B cells. To ensure that cluster 1 was not composed of B cells, we used Loupe Brower 4.0 to analyse the distributions in the expression of several B-cell marker genes in all the clusters. B-cell marker genes, such as *Cd79a*, *Cd79b*, and *Cd19*, were relatively highly expressed in B cells. (Fig. 4 A, left). However, the mice in the SiO_2-7d and NS-7d groups, and those in the SiO_2-56d and NS-56d groups, showed no detectable differences in the expression of these genes (Fig. 4 A, right). This finding indicates that B cells did not play a major role in pulmonary fibrosis, which was consistent with the results obtained using scRNA-seq and spatial transcriptomics (Fig. S2 M).

In contrast, genes encoding AT2 markers, such as *Sftpc, Sftpa1*, and *Sftpd* [31–32], were relatively highly expressed in cluster 1 (Fig. 4 B, left) and showed great upregulated expression levels in SiO_2-7d and SiO_2-56d mice (Fig. 4 B, right). *Scgb3a1* and *Scgb3a2*, which are markers of secretory epithelial or Club cells [33–34] (the progenitors of AT2 cells), were both expressed in AT2-like cluster 1 cells (Fig. 4 C, left). Spatially, *Scgb3a1* and *Scgb3a2* were expressed in the trachea (Fig. 4 C, right). The relatively increased expression levels of these 6 genes (*Sftpa1*, *Sftpb*, *Sftpc*, *Sftpd*, *Scgb3a1*, and *Scgb3a2*) in cluster 1 suggest that cluster 1 cells are alveolar progenitor cells of some kind.

Of these five genes, *Sftpa1*, *Sftpd*, and *Sftpc* showed higher activation in the SiO_2-56d mice than in the NS-56d mice (Fig. 4 B, right). Simultaneous assessment of *Igkv13-85* expression, and of that of the markers of AT2 and Club cells, revealed that more than half of *Igkv13-85*$^+$ cells co-expressed *Sftpc* (an AT2 cell marker) or *Scgb3a1* (a Club cell marker; Fig. 4 D); however, few *Igkv13-85*$^+$ cells co-expressed *Cd79a* or *Cd19* (Fig. 4 E). This result strongly suggests that these *Igkv13-85*$^+$ cells were not B cells. Based on these results, we speculated that cluster 1 represented a specialized type of alveolar epithelial cells type 2 (AT2 cells). Specifically, inhalation of silica could trigger the transformation of normal AT2 cells into *Igkv13-85*$^+$ AT2-like cells that could transcribe BCR genes.

The use of the V gene varies among different individuals. Expectedly, *Ighv1-64*, *Igkv13-85*, and *Igkv6-32* showed scant expression levels in the four sections obtained from our four groups of mice and used for spatial transcriptomic sequencing (Fig. S3 P). We next focused on *Igha*, a gene encoding the constant region of the immunoglobulin heavy chain that is crucial for determining the immunoglobulin isotype [30]. Similar to *Ighv1-64* and *Igkv13-85* (Fig. S3 Q), this gene was co-expressed with *Sftpc* (Fig. 4 F). Moreover, the expression of *Igha* in SiO_2-56d mice was much higher than that in the SiO_2-7d mice; this was consistent with the expansion of IgA-related clonotypes in SiO_2-56d mice (Fig. S3 E). The

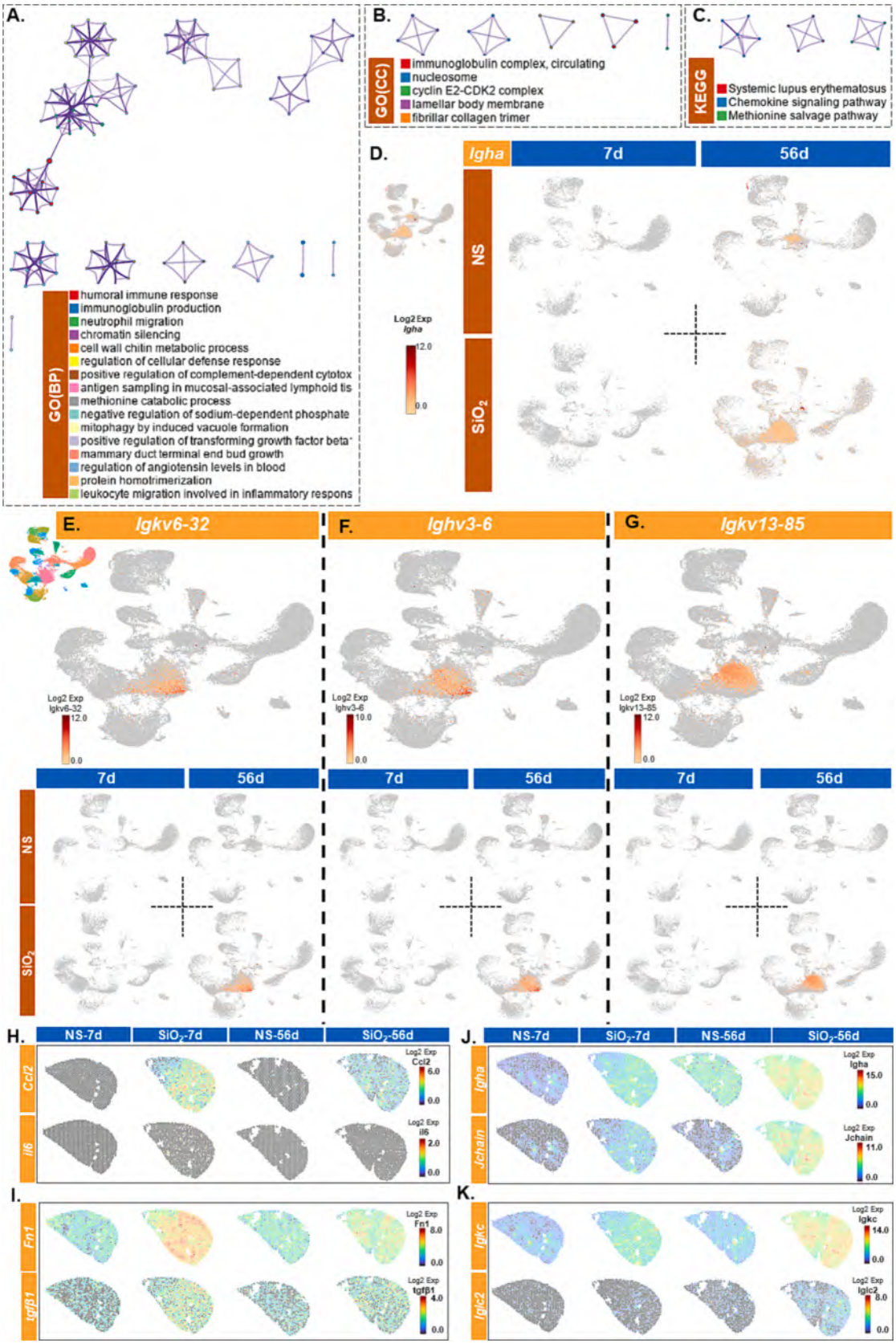

Fig. 2. Differentially expressed genes showing high expression levels in AT2-like cluster 1 cells are BCR genes. (A–C) GO and KEGG enrichment analysis of DEGs in cluster 1. Terms of interest are labelled in red. **(D)** Expression of *Igha* in the UMAP plot. **(E–G)** Expression of *Igkv6-32*, *Ighv3-6*, and *Igkv13-85* in the UMAP plot. The expression of each gene in the four samples is displayed individually. Colour bars indicate gene expression levels. **(H–K)** Corresponding gene expression levels in the four samples are shown. Scale bar = 1 mm. (H) *Ccl2* and *Il6* are related to inflammation; (I) *Fn1* and *Tgf-β1* are related to fibrosis; (J and K) *Igha*, *Jchain*, *Igkc*, and *Iglc2* are related to immunoglobulin production.

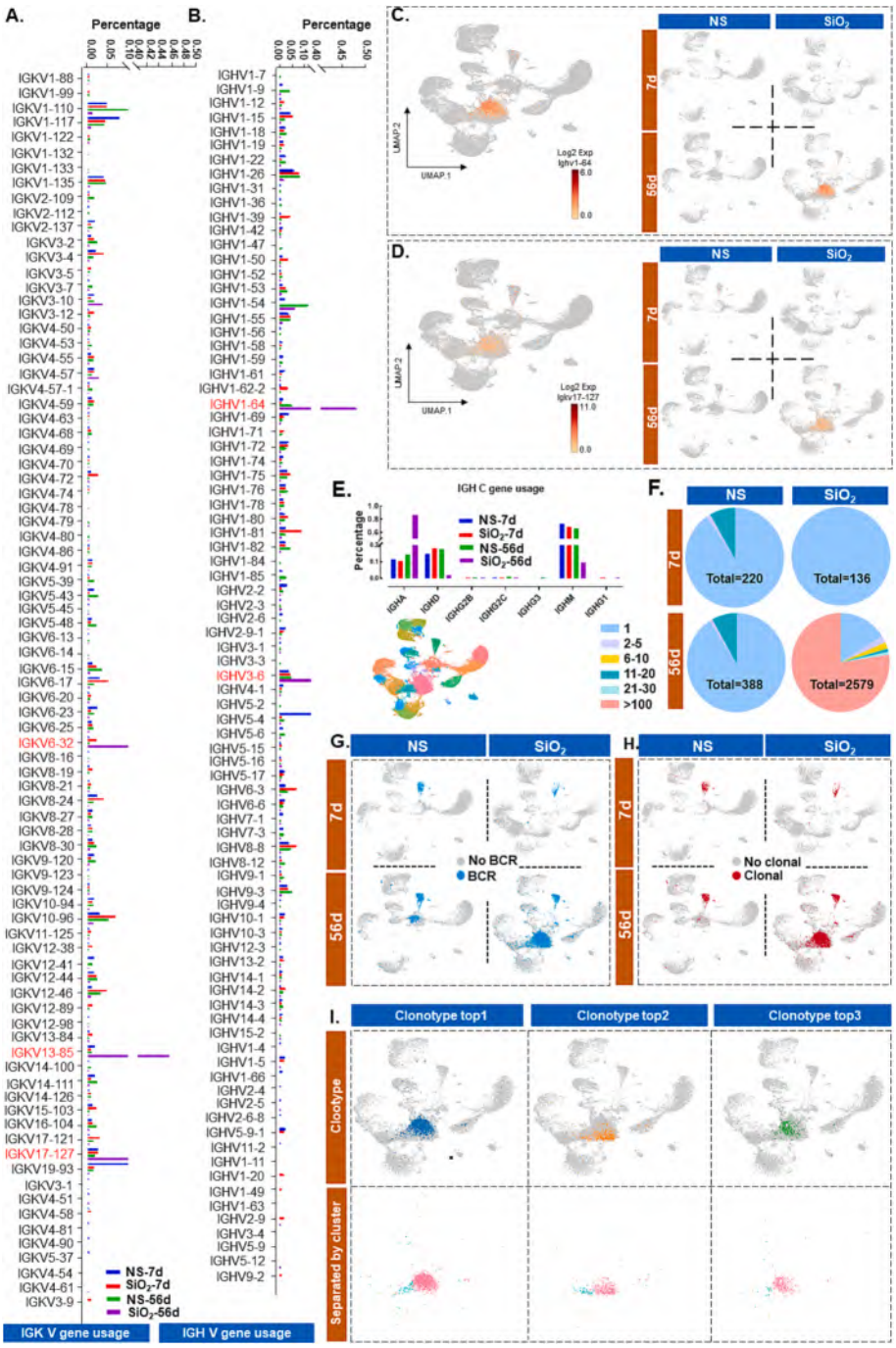

Fig. 3. BCR clonal expansion in SiO_2-56d mice. (A, B, and E) Usage of *Ighv* (A), *Igkv* (B), and *Ighc* (C) genes across SiO_2-7d, NS-7d, SiO_2-56d, and NS-56d mice. Different samples are designated using different colours. **(C)** Expression of *Ighv1-64* in the UMAP graph. **(D)** Expression of *Igkv17-127* in the UMAP graph. **(F)** Proportions of different clonotypes in SiO_2-7d, NS-7d, SiO_2-56d, and NS-56d mice. **(G)** UMAP of cells with BCR. The 24 clusters are indicated using different colours (top). **(H)** UMAP of cells with BCR clonotypes. **(I)** UMAP of cells having the top three clonotypes (top). Cells having the top three clonotypes merged with the 24 clusters (bottom). Pink represents cluster 1; blue represents cluster 15.

increased frequency of *Igha* use is common under pathologic conditions, and this finding indicates that the IgA-expressing AT2-like cell population may be important in pulmonary fibrosis.

To verify the presence of IgA-expressing AT2-like cells in the fibrotic lung tissue, we used RNAscope, a novel approach that can simultaneously detect multiple target RNAs in situ. Analysis using probes for the detection of *Igha* and *Sftpc* transcripts indicated that cells containing *Sftpc* transcripts were scattered throughout the NS-56d lung sections, and that these cells were normally located in the alveolar region (Fig. 4 G and Fig. S3 R). In the SiO_2-56d sections, *Sftpc*$^+$ cells tended to be crowded together. In the NS-56d sections, only a few cells contained *Igha* transcripts. Positivity for *Igha* was substantially increased in the SiO_2-56d sections, and *Igha* transcripts were colocalized with *Sftpc* transcripts within AT2-like cluster 1 cells. Based on these findings, we concluded that increased levels of *Igha* transcripts in the SiO_2-56d group were derived from AT2-like cluster 1 cells.

3.6. TCR expression is not amplified in SiO_2-7d or SiO_2-56d mice compared with that in NS-7d or NS-56d mice, respectively

T cells are primarily responsible for cellular immunity as opposed to humoral immunity. To evaluate the role of T-cell immunity in lung fibrosis, we reconstructed the TCR sequences for the SiO_2-7d, NS-7d, SiO_2-56d, and NS-56d mouse lung tissues from scRNA-seq. Our results indicate no differences in V(D)J and C gene usage among the four groups of mice (Fig. S4, A–F). The extent of clonal expansion in the four groups of mice showed that more than 80% of the clonotypes for each group were represented by only one cell (Fig. S4 G); the clonotype with the

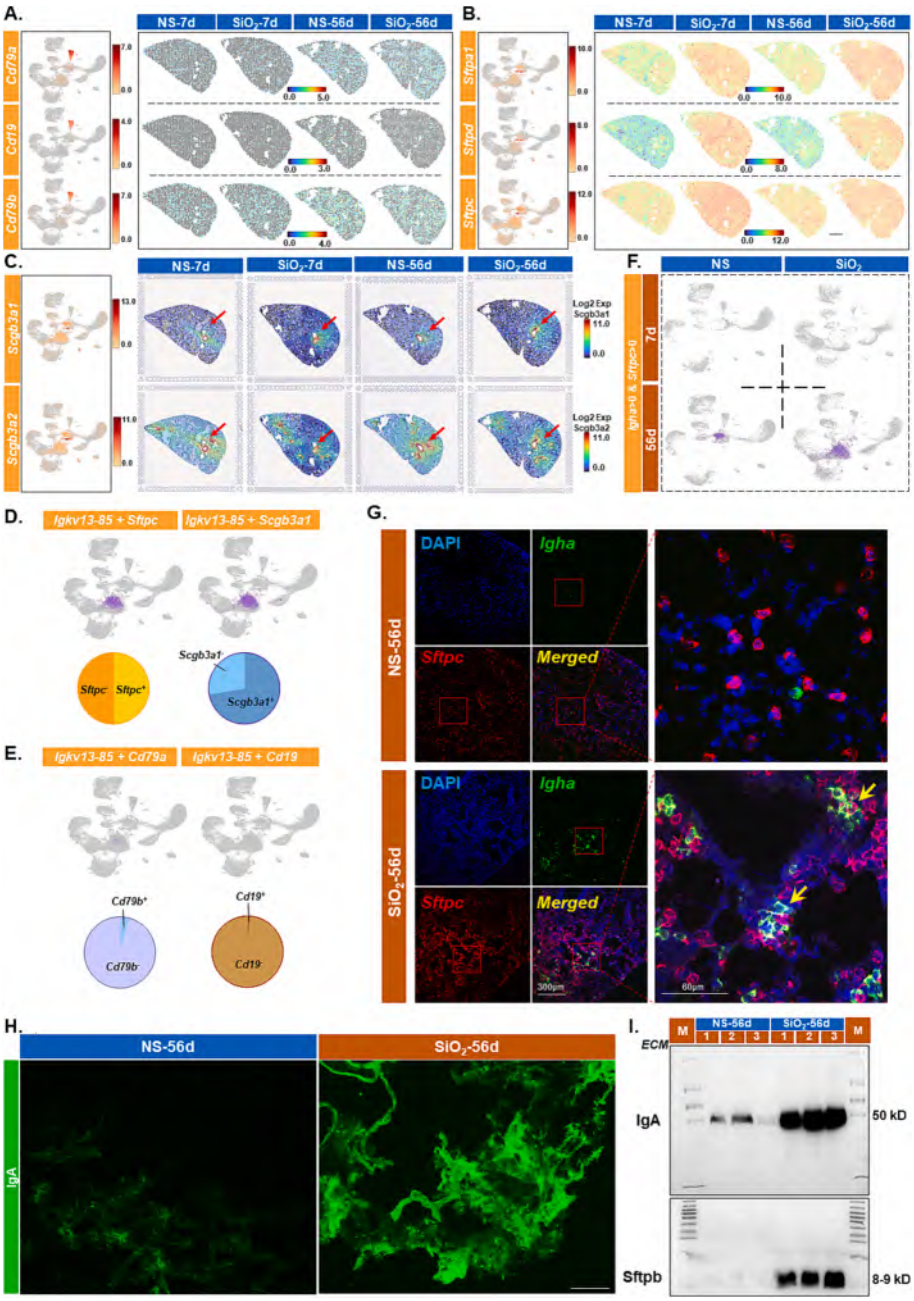

Fig. 4. Immunoglobulin-producing cluster 1 has more characteristics of AT2 cells than those of B cells. (A) Expression of *Cd79a*, *Cd19*, and *Cd79b* in the UMAP plot and sections of the four samples. Scale bar = 1 mm. **(B)** Expression of *Sftpa1*, *Sftpc*, and *Sftpd* in the UMAP plot and sections of the four samples. Scale bar = 1 mm. *Sftpa1*, *Sftpc*, and *Sftpd* were significantly increased in SiO_2-7d group versus NS-7 group and higher in SiO_2-56d group than NS-56d group. **(C)** Expression of *Scgb3a1* and *Scgb3a2* on the UMAP plot and sections of the four samples obtained from SiO_2-7d, NS-7d, SiO_2-56d, and NS-56d mice. Sections are merged with an image of H&E staining. Red arrows indicate tracheas with high expression of *Scgb3a1* or *Scgb3a2*. **(D and E)** UMAP plots show *Igkv13-85* coexpressed with *Sftpc*, *Scgb3a1*, *Cd79a*, and *Cd19*. Fan charts show the proportions of cells expressing corresponding genes in *Igkv13-85*$^{+}$ cells. **(F)** *Igha* is coexpressed with *Sftpc*. **(G)** *Igha* and *Sftpc* expression as detected by RNAscope. DAPI, blue; *Sftpc*, red; *Igha*, green. Magnified images of the regions in the red box are shown on the right. **(H)** Immunofluorescence shows immunoglobulin A (IgA) expression in the ECM. **(I)** Western blot of IgA expression in the ECM.

greatest expansion represented no more than 3% of all cells. The amino acid sequences of top 10 complementarity determining regions (CDR3) differed in the four groups of mice without a specific pattern or shared CDR sequences (Fig. S4 H). To explore the similarities and differences in clonotypes among the four groups of mice, we analysed the top 30 clonotypes for each group. Our results indicate that each group had a unique preferred clonotype, and no clonotype was shared among the four groups (Fig. S4 I). Then, we used Loupe (version 4.1.0, 10x Genomics) to integrate the barcodes of scRNA sequences and TCRs. The cells harbouring TCRs or paired clonotypes were recognized as T cells in each group, and there were no notable differences across the four groups (Fig. S4, J and K). Together, these findings indicate that there were no notable differences among the groups of mice, suggesting that T cells were not involved in lung fibrosis.

3.7. A large amount of immunoglobulin a is deposited into the fibrotic lung ECM

IgA deposits were found in the lung ECM of SiO_2-56d mice using immunofluorescence (Fig. 4 H) and western blotting (Fig. 4 I). To explore the components of ECM in the fibrotic lungs, we generated a decellularized lung matrix from SiO_2-56d ($n = 3$) and NS-56d ($n = 3$) mice, and analysed its protein components using mass spectrometry-based proteomics (Fig. 5 A). After analyzing the information collected, we identified 143 proteins with upregulated, and 127 proteins with downregulated, expression in the SiO_2-56d mice compared with those of the NS-56d mice (Fig. 7 A in [35]). Among these upregulated proteins, IgA showed the highest expression levels (Fig. 7B in [35]). Among the top 20 proteins with upregulated expression [35], the surfactant proteins SFTPB, SFTPD, and SFTPA are canonically considered to be secreted by mature AT2 cells [36]. Western blotting confirmed that the levels of IgA and SFTPB were substantially upregulated in the lung ECM of SiO_2-56d

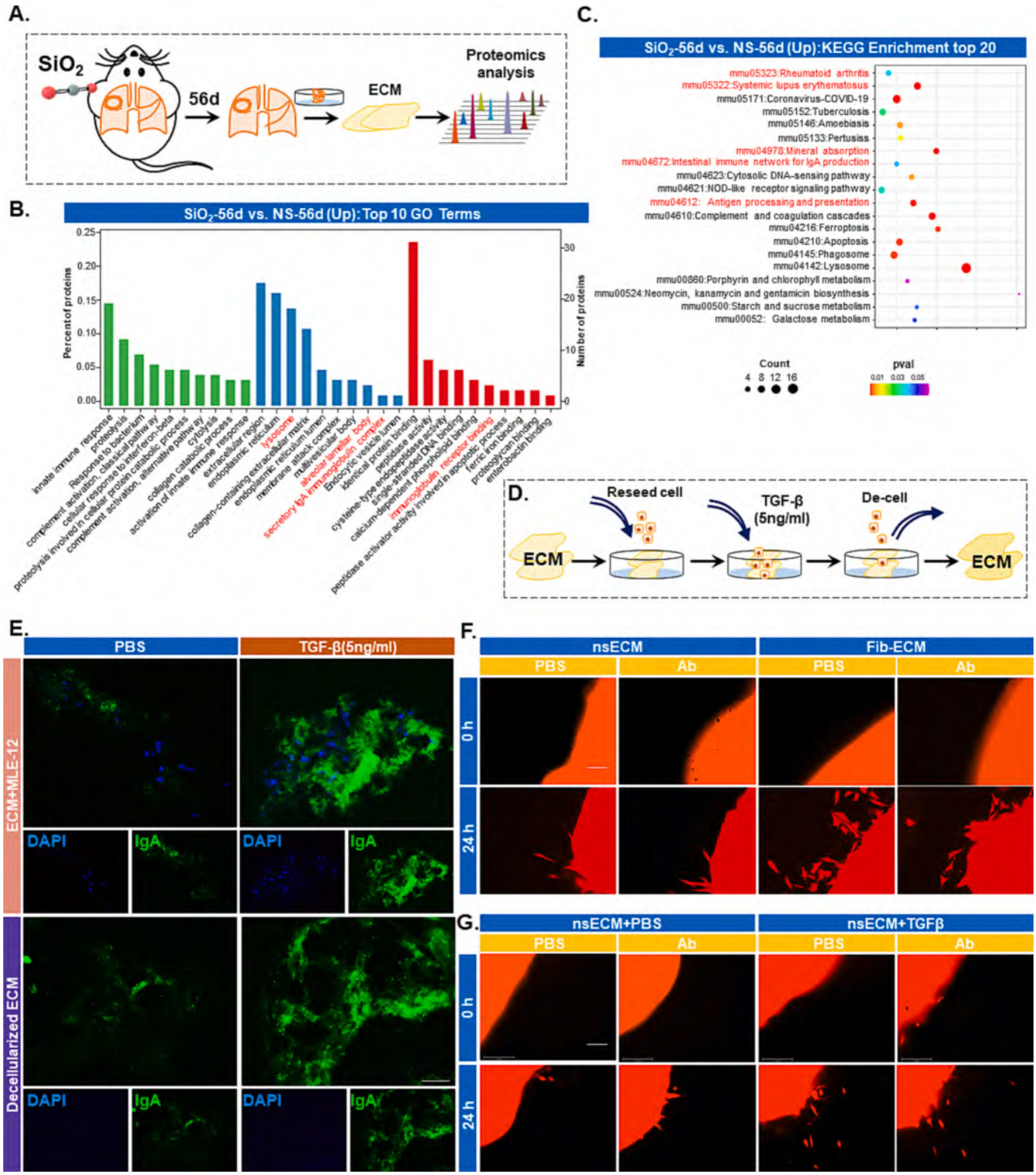

Fig. 5. IgA deposited into the ECM of SiO_2-56d mouse lungs activates fibroblasts. (A) Schematic diagram of ECM preparation. **(B and C)** Gene enrichment analyses of the DEGs designated in red. **(B)** Top 10 enriched GO terms, including BP, CC, and MC, are shown. Terms in red font are of particular interest. BP, biological process; CC, cellular component; MF, molecular function. **(C)** Top 20 KEGG enrichment terms. Terms in red are of particular interest in pulmonary fibrosis. **(D)** Schematic diagram for cell re-seeding procedure. **(E)** Representative immunofluorescence images of lung ECM. Scale bar = 50 μm. **(F and G)** Representative images of migration assays. nsECM, ECM obtained from mouse lung instilled with normal saline; FibECM, ECM obtained from mouse lung instilled with SiO_2 suspension for 56 days; Ab, anti-IgA antibody; 0 h, treated for 0 h; 24 h, treated for 24 h.

mice (Fig. 4 I). IgA deposition was accompanied by that of surfactant proteins, suggesting that IgA secretion may have been related to AT2 cells.

GO analysis of upregulated proteins in the SiO_2-56d mice identified lysosome, alveolar lamellar body, secretory IgA immunoglobulin complex, and immunoglobulin receptor binding as enriched terms (Fig. 5 B). KEGG analysis revealed pathways related to IgA production such as rheumatoid arthritis, systemic lupus erythematosus Top 10, and intestinal immune network (Fig. 5 C). In summary, these results indicate that lung fibrosis was closely associated with immunoglobulin production and AT2 cell function. Combined with the results of our sequencing analysis of the lung, these findings indicate a robust relationship between IgA expression and lung fibrosis.

3.8. Immunoglobulin a activates fibroblasts

TGF-β is a known pro-fibrotic factor that is commonly used to stimulate cells in the establishment of in-vitro models of fibrosis. Here, we cultured MLE-12 cells, which are mouse lung epithelial cells having the characteristics of AT2 cells. MLE-12 cells were treated using TGF-β at different time points. Our results show that the expression of Igha mRNA was upregulated at 72 h post-treatment with TGF-β (Fig. S5 A). Then, we evaluated IgA expression levels using western blotting. Using an antibody specific for IgA, we detected a band at 75 kDa, which was equal to the total molecular weight of the light and heavy chains of IgA (Fig. S5 B). The intensity of this band increased after the MLE-12 cells were treated with TGF-β for 72 h. To verify that MLE-12 cells could secrete IgA into the lung ECM, we seeded MLE-12 cells into the ECM obtained from healthy mouse lungs; then, we treated this seeded ECM with TGF-β. Next, we decellularized this lung ECM by removing the MLE-12 cells, and evaluated IgA expression in this ECM using immunofluorescence and western blotting (Fig. 5 D). Our results indicate an increased expression of IgA in the lung ECM treated using TGF-β compared with that of control ECM (Fig. 5 E and Fig. S5 C). This finding indicates that the lung epithelium secreted IgA into the lung ECM.

To explore the effects of IgA deposition in the ECM on fibroblasts, we seeded MLg cells (a mouse lung fibroblast cell line) into ns- or Fib-ECM, which were then cultured with or without an anti-IgA antibody. Migration assays showed that Fib-ECM promoted an increase in the number of migrated MLg cells and increased their migration distance. This effect was inhibited by anti-IgA antibody (Fig. 5 F and Fig. S5, D–F). Next, we seeded MLg cells onto a lung ECM that had been previously cultured with MLE-12 cells with or without treatment using TGF-β. Then, we treated this ECM with an anti-IgA antibody. Our results indicate that MLg cells showed an increased number of migrations and migration distance into the ECM that had been cultured with MLE-12 cells and treated using TGF-β (Fig. 5 G and Fig. S5 G–I). An anti-IgA antibody could partially block the facilitation of migration in MLg cells. These findings indicate that secretion of IgA into the ECM by MLE-12 cells promoted the activation and migration of fibroblasts, which may have contributed to the fibrotic process.

4. Discussion

IPF is a type of pulmonary interstitial fibrotic disease [37]. Patients with IPF experience a decline in pulmonary function, which greatly affects their quality of life and shortens life span [38]. Nintedanib and pirfenidone, which are the only drugs currently approved for the clinical treatment of pulmonary fibrosis, cannot reverse the fibrosis that has already occurred or prolong the life of patients with IPF [39–40]. Interstitial fibrosis is directly caused by increased secretion of collagen by activated pulmonary fibroblasts [41]. In this study, we demonstrated in vitro that IgA deposited on ECM can promote the migration of fibroblast cell migration. Its molecular mechanism deserves further research to provide a target for inhibiting the activation of fibroblasts, which is a limitation of this research. In recent years, an increasing number of studies have indicated that injury to, or changes in the gene expression of, lung alveolar epithelial cells are the initiating factors of pulmonary fibrosis [7,10,42]. In addition, studies have shown that immune system disorders are associated with pulmonary fibrosis [43–45]. Patients with immune system diseases, such as systemic lupus erythematosus (SLE) or cystic fibrosis, have increased concentrations of IgA in blood, which is related to the severity of pulmonary fibrosis [18,46]. The Fc segment receptor for IgA can activate neutrophils and macrophages [47]; studies have also shown that it can activate pulmonary fibroblasts and promote pulmonary fibrosis [16]. However, the relationship between lung epithelium and IgA has not been investigated. Because IgA can activate lung fibroblasts, it is important to uncover the cell sources and routes of IgA secretion and deposition. In our present study, we have shown that lung alveolar epithelial cells were the direct sources of pulmonary IgA production. This finding provides possible future therapeutic targets for blocking IgA secretion in the lung.

In this study, we used intratracheal instillation of silica to establish a mouse model of pulmonary fibrosis. Whole lung cells, lung tissue sections, and lung ECM were respectively analyzed using single cell sequencing, space transcriptome sequencing, and proteomics. Our comprehensive and muti-omics analysis showed a cluster that contained AT2-like cells in the fibrotic lung. These AT2-like cells could secrete a large amount of IgA, which was enriched in the fibrotic lung ECM. In-vitro experiments showed that IgA enriched in the lung ECM contributed to pulmonary fibrosis. In recent years, studies have shown that senescence of AT2 cells and their ability to secrete cytokines participate in the initiation of pulmonary fibrosis [9]. The results obtained in our present study have confirmed that AT2-like cells had the potential to secrete IgA via BCR rearrangement. We confirmed these results at mRNA level using single-cell sequencing and BCR rearrangement analysis. Increased levels of IgA, which are found in the blood of patients with cystic fibrosis, can activate pulmonary fibroblasts [18]. This finding agrees with the results obtained in our present study, which show that IgA could increase the activity of MLg cells and promote their migration. However, in our model, the IgA deposited into the ECM originated from local lung cells and not from blood. Because we directly sequenced and analyzed whole lung cells, we found that the AT2-like cluster 1 cells were highly clonal for BCR.

The development of single-cell sequencing technology has made it possible to analyze the immune repertoire has been more accurately, and the diversity and amplification of BCR sequences in diseases have been explored [48–49]. In research into the BCR repertoire of human blood mononuclear cells, the use frequency of Ighv3-53 in SLE groups has been reported to be as high as 6.23%, vs 2.46% in HC groups. Ighv3-33 in SLE groups has been reported to be 14.46%, vs 4.62% in HC groups. This is considered to be of pathological significance [50]. In our study, the use frequency of Igkv13-85 in the SiO2-56d group was 45.35% vs 1.08% in our NS-56d group. The number of clonal cells to which Igkv13-85 belongs accounted for 47.8% of the total BCR clone cells. Therefore, the BCR clonal cell expansion in our study should be considered to have important pathological significance. In recent years, there have been even more studies based on single-cell sequencing and BCR/TCR. The degree of amplification of BCR monoclonal cells in the present work, reaching 47.8%, is the highest ever reported. Collectively, BCR clonal cells account for a considerable proportion of whole lung cells, which suggests that these cells may dominate the development of lung diseases.

Pseudotime analysis indicated that cluster 1, 3, and 15 cells had lineage relationships. However, AT2 can differentiate from other airway epithelial stem cells and can undergo self-renewal and differentiation in vivo [51]. The lineage sources of these three clusters of cells and the mechanism of silica-induced differentiation are worth further research. From another perspective, AT2-like cluster 1 cells exist in lungs instilled with silica suspension and not in normal lungs, which can also be understood, as silica induces IgA expression in AT2 cells. Because AT2 cells tend to readily differentiate into AT1 cells in vitro, we did not isolate

AT2-like cells from our silica-induced mice for primary culture. In our future studies, we will aim to improve our methodology for the in-vitro culture of primary AT2-like cells in order to preserve the AT2-like characteristics of these cells. We will also further verify and investigate BCR rearrangement in AT2-like cells using various mouse models of, and samples obtained from patients with pulmonary fibrosis.

It has been suggested that in the next 10 years [52], idiopathic pulmonary fibrosis will be reclassified as epithelial-driven pulmonary fibrosis, primary pulmonary fibrosis, or progressive age-dependent pulmonary fibrosis. Based on this possibility, and on our present findings showing that AT2-like cells secreted IgA into the fibrotic lung ECM, we will investigate other types of pulmonary fibrosis and classify them according to the presence or absence of IgA deposition into the lung. Using ablation of over-proliferating AT2-like cells or blocking the production of IgA in these cells may become a potential therapeutic target in the treatment of patients with pulmonary fibrosis.

In conclusion, a cluster of AT2-like cells was found to obtain BCR transcripts in the silica-induced fibrotic lung, which is related to IgA. At the same time, a large amount of IgA was found in lung ECMs of fibrotic lungs. Our study indicates that the lung is an organ with huge immune function which can be activated when the lung is subjected to certain stimuli. IgA produced by lung resident cells is closely related to the occurrence of pulmonary fibrosis. In addition, IgA in the steady-state maintenance of alveolar structure and function is worthy of further exploration.

5. Online supplemental material

Fig. S1 presents the validation of the pulmonary fibrosis model and the marker gene and proportion of each cell cluster. Fig. S2 presents the enrichment analysis of upregulated genes of macrophages at the inflammatory stage. Combined analysis of scRNA-seq and space transcriptomics predicted the accumulation of macrophages in the area of inflammation of the SiO_2-7d sample. Fig. S3 presents the usage and pairing of BCR genes in the four samples obtained from SiO_2-7d, NS-7d, SiO_2-56d, and NS-56d mice. Fig. S4 presents no clonal expansion of T cells in any of the four samples obtained from SiO_2-7d, NS-7d, SiO_2-56d, and NS-56d mice. Fig. S5 depicts that MLE-12 cells produce IgA to activate MLg cells.

Declaration of Competing Interest

The authors declare that they have no known competing financial interests or personal relationships that could have appeared to influence the work reported in this paper.

Data availability

Data will be made available on request.

Acknowledgments

This study is the result of work that was partially supported by resources and facilities at the Core Laboratory at the Medical School of Southeast University. This work was supported by The National Key R&D Program of China (2022YFC2504403), The National Natural Science Foundation of China (81972987, 81773796, 81700068, and 81803182) and the Jiangsu Provincial Key Laboratory of Critical Care Medicine (JSKLCCM-2022-02-005). We thank LetPub (www.letpub.com) for linguistic assistance and pre-submission expert review.

Author contributions.

Author contributions: M. Chen, J. Wang, and M. Yuan performed the experiments, interpreted the data, prepared the figures, and wrote the manuscript. M. Long, Y. Sun, S. Wang, W. Luo, Y. Zhou, and W. Zhang performed the experiments and interpreted the data. W. Jiang designed the experiments, interpreted the data, and wrote the manuscript. J. Chao provided laboratory space and funding, designed the experiments, interpreted the data, wrote the manuscript, and directed the project. All the authors read, discussed, and approved the final version of the manuscript.

Disclosures: The authors declare no competing financial interests.

Appendix A. Supplementary material

Supplementary data to this article can be found online at https://doi.org/10.1016/j.intimp.2023.110545.

References

[1] P.W. Noble, C.E. Barkauskas, D. Jiang, Pulmonary fibrosis: patterns and perpetrators, J. Clin. Invest. 122 (2012) 2756–2762, https://doi.org/10.1172/JCI60323.
[2] S.E. McGowan, Extracellular matrix and the regulation of lung development and repair, FASEB J. 6 (1992) 2895–2904, https://doi.org/10.1096/fasebj.6.11.1644255.
[3] A.D. Theocharis, S.S. Skandalis, C. Gialeli, N.K. Karamanos, Extracellular matrix structure, Adv. Drug Deliv. Rev. 97 (2016) 4–27, https://doi.org/10.1016/j.addr.2015.11.001.
[4] V.J. Thannickal, G.B. Toews, E.S. White, J.P. Lynch Iii, F.J. Martinez, Mechanisms of pulmonary fibrosis, Annu. Rev. Med. 55 (2004) 395–417, https://doi.org/10.1146/annurev.med.55.091902.103810.
[5] Q. Liu, et al., Lung regeneration by multipotent stem cells residing at the bronchioalveolar-duct junction, Nat. Genet. 51 (2019) 728–738, https://doi.org/10.1038/s41588-019-0346-6.
[6] C.E. Barkauskas, et al., Type 2 alveolar cells are stem cells in adult lung, J. Clin. Invest. 123 (2013) 3025–3036, https://doi.org/10.1172/JCI68782.
[7] J. Katzen, M.F. Beers, Contributions of alveolar epithelial cell quality control to pulmonary fibrosis, J. Clin. Invest. 130 (2020) 5088–5099, https://doi.org/10.1172/JCI139519.
[8] D.J. Lederer, F.J. Martinez, Idiopathic pulmonary fibrosis, N. Engl. J. Med. 378 (2018) 1811–1823, https://doi.org/10.1056/nejmra1705751.
[9] C. Yao, et al., Senescence of alveolar type 2 cells drives progressive pulmonary fibrosis, Am. J. Respir. Crit. Care Med. 203 (2021) 707–717, https://doi.org/10.1164/rccm.202004-1274OC.
[10] T. Parimon, C. Yao, B.R. Stripp, P.W. Noble, P. Chen, Alveolar epithelial type II cells as drivers of lung fibrosis in idiopathic pulmonary fibrosis, Int. J. Mol. Sci. 21 (2020) 2269, https://doi.org/10.3390/ijms21072269.
[11] I.J. Amanna, M.K. Slifka, Contributions of humoral and cellular immunity to vaccine-induced protection in humans, Virology 411 (2011) 206–215, https://doi.org/10.1016/j.virol.2010.12.016.
[12] E. Moga, E. Lynton-Pons, P. Domingo, The robustness of cellular immunity determines the fate of SARS-CoV-2 infection, Front. Immunol. 13 (2022), 904686, https://doi.org/10.3389/fimmu.2022.904686.
[13] M.B. Horton, E.D. Hawkins, S. Heinzel, P.D. Hodgkin, Speculations on the evolution of humoral adaptive immunity, Immunol. Cell Biol. 98 (2020) 439–448, https://doi.org/10.1111/imcb.12323.
[14] R. Levin-Klein, Y. Bergman, Epigenetic regulation of monoallelic rearrangement (allelic exclusion) of antigen receptor genes, Front. Immunol. 5 (2014) 625, https://doi.org/10.3389/fimmu.2014.00625.
[15] A. Breedveld, M. van Egmond, IgA and FcαRI: Pathological roles and therapeutic opportunities, Front. Immunol. 10 (2019) 553, https://doi.org/10.3389/fimmu.2019.00553.
[16] S. Arakawa, et al., Secretory immunoglobulin A induces human lung fibroblasts to produce inflammatory cytokines and undergo activation, Clin. Exp. Immunol. 195 (2019) 287–301, https://doi.org/10.1111/cei.13253.
[17] P. Heukels, et al., Enhanced Bruton's tyrosine kinase in B-cells and autoreactive IgA in patients with idiopathic pulmonary fibrosis, Respir. Res. 20 (2019) 232, https://doi.org/10.1186/s12931-019-1195-7.
[18] R. Yadav, et al., IgA autoantibodies directed against self DNA are elevated in cystic fibrosis and associated with more severe lung dysfunction, Autoimmunity 53 (2020) 476–484, https://doi.org/10.1080/08916934.2020.1839890.
[19] A.M. Collin, et al., Lung immunoglobulin A immunity dysregulation in cystic fibrosis, EBioMedicine 60 (2020), 102974, https://doi.org/10.1016/j.ebiom.2020.102974.
[20] R.M. Mauch, et al., Secretory IgA response against Pseudomonas aeruginosa in the upper airways and the link with chronic lung infection in cystic fibrosis. Pathog. Dis. 75, ftx069, doi:10.1093/femspd/ftx069 (2017).
[21] H. Liu, et al., Macrophage-derived MCPIP1 mediates silica-induced pulmonary fibrosis via autophagy, Part. Fibre Toxicol. 13 (2016) 55, https://doi.org/10.1186/s12989-016-0167-z.
[22] Z. Zhou, et al., circRNA mediates silica-induced macrophage activation via HECTD1/ZC3H12A-dependent ubiquitination, Theranostics 8 (2018) 575–592, https://doi.org/10.7150/thno.21648.
[23] X. Shi, et al., GREM1/PPP2R3A expression in heterogeneous fibroblasts initiates pulmonary fibrosis, Cell Biosci. 12 (2022) 123, https://doi.org/10.1186/s13578-022-00860-0.

[24] X. Zhang, et al., Cell Marker: a manually curated resource of cell markers in human and mouse, Nucl. Acids Res. 47 (2019) D721–D728, https://doi.org/10.1093/nar/gky900.
[25] S. Tan, S. Chen, Macrophage autophagy and silicosis: current perspective and latest insights, Int. J. Mole. Sci. 22 (2021) 453, https://doi.org/10.3390/ijms22010453.
[26] P.X. Liew, P. Kubes, The neutrophil's role during health and disease, Physiol. Rev. 99 (2019) 1223–1248, https://doi.org/10.1152/physrev.00012.2018.
[27] M. Asp, et al., A spatiotemporal organ-wide gene expression and cell atlas of the developing human heart, Cell 179 (2019) 1647–1660.e1619, https://doi.org/10.1016/j.cell.2019.11.025.
[28] R. Melo Ferreira, et al., Integration of spatial and single-cell transcriptomics localizes epithelial cell-immune cross-talk in kidney injury, JCI Insight 6 (2021) e147703.
[29] G. Babbage, C.H. Ottensmeier, J. Blaydes, F.K. Stevenson, S.S. Sahota, Immunoglobulin heavy chain locus events and expression of activation-induced cytidine deaminase in epithelial breast cancer cell lines, Cancer Res. 66 (2006) 3996–4000, https://doi.org/10.1158/0008-5472.can-05-3704.
[30] N. Kumar, C.P. Arthur, C. Ciferri, M.L. Matsumoto, Structure of the secretory immunoglobulin A core, Science 367 (2020) 1008–1014, https://doi.org/10.1126/science.aaz5807.
[31] X. Han, et al., Mapping the mouse cell atlas by Microwell-Seq, Cell 172 (2018) 1091–1107.e1017, https://doi.org/10.1016/j.cell.2018.02.001.
[32] A. Jacob, et al., Differentiation of human pluripotent stem cells into functional lung alveolar epithelial cells, Cell Stem Cell 21 (2017) 472–488.e410, https://doi.org/10.1016/j.stem.2017.08.014.
[33] X. Naizhen, T. Kido, S. Yokoyama, R.I. Linnoila, S. Kimura, Spatiotemporal expression of three secretoglobin proteins, SCGB1A1, SCGB3A1, and SCGB3A2, in mouse airway epithelia, J. Histochem. Cytochem. 67 (2019) 453–463, https://doi.org/10.1369/0022155419829050.
[34] S.D. Reynolds, P.R. Reynolds, G.S. Pryhuber, J.D. Finder, B.R. Stripp, Secretoglobins SCGB3A1 and SCGB3A2 define secretory cell subsets in mouse and human airways, Am. J. Respir. Crit. Care Med. 166 (2002) 1498–1509, https://doi.org/10.1164/rccm.200204-285oc.
[35] J. Yin, et al., A missing piece of the puzzle in pulmonary fibrosis: anoikis resistance promotes fibroblast activation, Cell Biosci. 12 (2022) 21, https://doi.org/10.1186/s13578-022-00761-2.
[36] Y. Yamamoto, et al., Long-term expansion of alveolar stem cells derived from human iPS cells in organoids, Nat. Methods 14 (2017) 1097–1106, https://doi.org/10.1038/nmeth.4448.
[37] K.C. Meyer, Pulmonary fibrosis, part I: Epidemiology, pathogenesis, and diagnosis, Expert Rev. Respir. Med. 11 (2017) 343–359, https://doi.org/10.1080/17476348.2017.1312346.
[38] F.J. Martinez, et al., Idiopathic pulmonary fibrosis, Nat. Rev. Dis. Primers 3 (2017) 17074, https://doi.org/10.1038/nrdp.2017.74.
[39] L. Richeldi, et al., Efficacy and safety of nintedanib in idiopathic pulmonary fibrosis, N. Engl. J. Med. 370 (2014) 2071–2082, https://doi.org/10.1056/nejmoa1402584.
[40] T.M. Maher, et al., Pirfenidone in patients with unclassifiable progressive fibrosing interstitial lung disease: a double-blind, randomised, placebo-controlled, phase 2 trial, Lancet Respir. Med. 8 (2020) 147–157, https://doi.org/10.1016/s2213-2600(19)30341-8.
[41] P.J. Wolters, H.R. Collard, K.D. Jones, Pathogenesis of idiopathic pulmonary fibrosis, Annu. Rev. Pathol. 9 (2014) 157–179, https://doi.org/10.1146/annurev-pathol-012513-104706.
[42] Y. Tian, et al., Loss of PTEN induces lung fibrosis via alveolar epithelial cell senescence depending on NF-κB activation, Aging Cell 18 (2019) e12858.
[43] P. Heukels, C.C. Moor, J.H. von der Thüsen, M.S. Wijsenbeek, M. Kool, Inflammation and immunity in IPF pathogenesis and treatment, Respir. Med. 147 (2019) 79–91, https://doi.org/10.1016/j.rmed.2018.12.015.
[44] J. Dong, Q. Ma, Type 2 immune mechanisms in carbon nanotube-induced lung fibrosis, Front. Immunol. 9 (2018) 1120, https://doi.org/10.3389/fimmu.2018.01120.
[45] L. Turner-Stokes, et al., Autoantibody and idiotype profile of lung involvement in autoimmune rheumatic disease, Ann. Rheum. Dis. 49 (1990) 160–162, https://doi.org/10.1136/ard.49.3.160.
[46] S. Palmucci, et al., Clinical and radiological features of lung disorders related to connective-tissue diseases: a pictorial essay, Insights Imag. 13 (2022) 108, https://doi.org/10.1186/s13244-022-01243-2.
[47] M. van Egmond, et al., IgA and the IgA Fc receptor, Trends Immunol. 22 (2001) 205–211, https://doi.org/10.1016/s1471-4906(01)01873-7.
[48] P. Wang, et al., Global characterization of peripheral B cells in Parkinson's disease by single-cell RNA and BCR sequencing, Front. Immunol. 13 (2022), 814239, https://doi.org/10.3389/fimmu.2022.814239.
[49] J. Ma, et al., Novel skewed usage of B-cell receptors in COVID-19 patients with various clinical presentations, Immunol. Lett. 249 (2022) 23–32, https://doi.org/10.1016/j.imlet.2022.08.006.
[50] Y. Zhang, T.-Y. Lee, Revealing the immune heterogeneity between systemic lupus erythematosus and rheumatoid arthritis based on multi-omics data analysis, Int. J. Mol. Sci. 23 (2022) 5166, https://doi.org/10.3390/ijms23095166.
[51] B. Jones-Freeman, M.R. Starkey, Bronchioalveolar stem cells in lung repair, regeneration and disease, J. Pathol. 252 (2020) 219–226, https://doi.org/10.1002/path.5527.
[52] A.U. Wells, K.K. Brown, K.R. Flaherty, M. Kolb, V.J. Thannickal, What's in a name? That which we call IPF, by any other name would act the same, Euro. Respir. J. 51 (2018), https://doi.org/10.1183/13993003.00692-2018.